Utilizing spectral induced polarization to identify the ice core of a pingo: A case study in Haines Junction, Yukon, Canada

Hosein Fereydooni[1], Stephan Gruber[2], Derek Cronmiller[3] & David Stillman[4]

[1]*Department of Earth Sciences, Carleton University, Ottawa, Ontario, Canada*

[2]*Department of Geography and Environmental Studies, Carleton University, Ottawa, Ontario, Canada*

[3]*Permafrost Geologist, Energy, Mines and Resources, Yukon Geological Survey, Yukon, Canada*

[4]*Southwest Research Institute, Boulder, Colorado, United States*

ABSTRACT

This paper presents a field study conducted in Haines Junction, Yukon, utilizing Spectral Induced Polarization (SIP) to investigate the subsurface properties of a pingo site and specifically identify its ice core. The effectiveness of SIP analysis was demonstrated using a FUCHS frequency domain instrument, which measured electrical impedance magnitude and phase shift angle at multiple frequencies (1.46 Hz–40 kHz). The main focus of the analysis centered on the results obtained from electrical impedance magnitude and phase shift angle inversion at 40 kHz and 1.46 Hz. The inversion results revealed the presence of high resistivity layers within the subsurface, similar to results that would be expected with electrical resistivity tomography (ERT). Additionally, the SIP data revealed that some areas with high resistivity also had negative phase shift angle values, suggesting the presence of materials with polarizing properties. The analysis of the imaginary part of electrical impedance at 40 kHz for these areas highlighted the contribution of polarization, indicating the presence of ice. Furthermore, the electrical impedance magnitude at 1.46 Hz exhibited similarities to the 40 kHz analysis, but with higher resistivity. This pattern is another indicator of the presence of ice within the subsurface of the study area and was expressed using the Resistivity Frequency Effect (RFE) equation. The RFE analysis and the patterns of polarization confirmed the presence of the pingo ice core and identified its distinctive signature compared to other layers. Subsequent drilling confirmed the presence of interbedded ice and clay from 2.4–3.6 m depth and massive ice from 3.6–8.3 m depth.

1 INTRODUCTION

Permafrost is an integral component of Earth's subsurface in cold regions and encompasses a substantial volume of ground ice. Especially under climate change, melting of ground ice can give rise to various hazards, making the detection and understanding of ice within permafrost important for prevention and mitigation of associated problems. In this context, geophysical methods provide tools for detecting and characterizing ground ice.

Among the methods commonly used, ERT has been widely employed to investigate permafrost (e.g., You et al. 2013; Oldenborger 2021; Li et al. 2021; Park et al. 2023; Kasprzak et al. 2017). However, distinguishing ice from other materials via ERT alone can be challenging when resistivity values overlap between frozen ground and, for example, unfrozen bedrock. As a result, investigating alternative techniques that can detect ice with less ambiguity is important.

Spectral Induced Polarization (SIP) is a promising method for characterizing ground ice. Under Alternating Current (AC), ice and frozen soil exhibit polarization, that can be detected with SIP. The spectral signature of this polarization is linked to ice content, temperature, and salinity. While field application of SIP for detecting ground ice is only beginning, several studies have demonstrated success.

Running SIP field measurements above conductive layers such as an unfrozen and wet active layer presents significant challenges (Stillman et al. 2018). In areas with highly conductive subsurface materials, especially saline or clay-rich soils, the electrical currents tend to concentrate within these layers, leading to signal attenuation and limited penetration depth. This can result in reduced resolution and difficulties in distinguishing responses from specific target zones at depth. Additionally, clay minerals in the subsurface introduce capacitive and conductive responses (Bittelli et al. 2004). That can mask or interfere with the signature of ice or other target materials. Measurements in late winter can minimize these effects as the active layer will be maximally frozen.

Numerous processing techniques can be applied to SIP data. Initial steps involve the separation of real and imaginary parts. The imaginary part and phase shift angle reflect polarization, which can provide a signature diagnostic of ice. Data can be processed across multiple frequencies, employing equations such as the Resistivity Frequency Effect (RFE), which can enhance the clarity of ice detection.

The objective of this research is to improve and demonstrate the potential of SIP in detecting ground ice using late-winter measurements over a pingo as a case study.

First, we give a brief background and explain the methods employed to analyze our data. Subsequently, inversion was employed to compare the results with evidence obtained from logged borehole cores, considering various perspectives.

https://doi.org/10.52381/ICOP2024.211.1

2 BACKGROUND

2.1 The Dielectric Behaviour of Ice

When materials are exposed to an electric field, individual molecules are polarized by electron or proton displacements and slight molecular distortions. In ice, polarization arises from the reorientation of molecules or bonds. Certain proton configurations experience reduced energies compared to others, resulting in a net polarization of the ice at thermal equilibrium. This polarization at low frequencies is an almost perfect example of Debye relaxation (Grimnes and Martinsen 2015). While a consistent flow of current in accordance with Ohm's law can be induced in ice, it is driven by the movement of protons (Petrenko and Whitworth 1999) rather than the common electronic conduction.

Generally, electronic and atomic polarization are characterized by a resonance frequency, causing a peak in the imaginary part and a peak followed by a trough in the real part of permittivity. Conversely, ionic, interfacial, and dipolar polarizations are characterized by a relaxation frequency, which manifests as a decrease in the real part of permittivity and a peak in the imaginary part.

To extract the relaxation frequency of frozen soil and ice we can consider an equivalent circuit to simulate their electrical manner (Hobbs 2010). In this respect, we can apply the Debye equation to the result of dielectric spectra and extract the relaxation frequency for ice and frozen soil [Equations 1 and 2].

$$\varepsilon'(\omega) = \varepsilon_\infty + \frac{\Delta\varepsilon}{1+\omega^2\tau^2} \quad [1]$$

$$\varepsilon''(\omega) = \varepsilon_\infty + \frac{\Delta\varepsilon\omega\tau}{1+\omega^2\tau^2} \quad [2]$$

Where ε' is real permittivity (or dielectric constant), and ε'' imaginary permittivity (or loss factor). ε_{LF}, ε_∞ is low, and high frequency permittivity, and $\Delta\varepsilon = \varepsilon_{LF} - \varepsilon_\infty$.

At a temperature of +10 °C, water demonstrates an approximate relaxation time of $\tau = 1.2 \times 10^{-11}$ s, while ice at -10 °C exhibits a relaxation time of approximately $\tau = 5 \times 10^{-5}$ s (Petrenko and Whitworth 1999).

2.2 The Dielectric Behaviour of Frozen Soil

Frozen soil has significant variations in dielectric permittivity across frequency. At lower frequencies, there can be a pronounced increase in permittivity, potentially attributable to surface mineral polarization. At frequencies below 1 kHz, the polarization effect primarily stems from electrochemical (ionic) polarization occurring at the interface between the pore water and the solid matrix, known as the electrical double layer (EDL; Kemna et al. 2012). Particle size plays a pivotal role, with lower frequencies (< 1 kHz) witnessing considerable permittivity increases as particle size decreases, owing to factors like Maxwell-Wagner effects, surface conduction, ion exchange, and interface polarization, particularly prominent in clay-rich soils. Relaxation frequency increases with rising temperature. Water's proximity to solid surfaces also affects relaxation frequencies, with closer water molecules displaying lower-frequency relaxations. These observations suggest that the dielectric behavior of frozen soil arises from several relaxations, including those related to ice and adsorbed unfrozen water, as supported by Debye parameterization results (Bittelli et al. 2004; Grimm et al. 2015). Figure 1 shows the dielectric spectra for water and ice. The relaxation frequency (the peaks in the imaginary part) for ice (and frozen soil) occurs at a lower frequency than water.

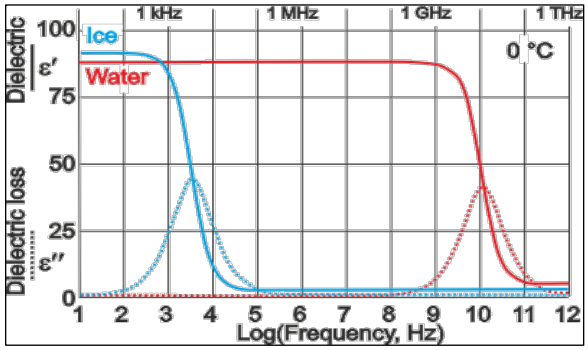

Figure 1. Relaxation frequency for ice (blue line) and water (red line) at 0 °C (Artemov and Volkov 2014).

2.3 Spectral Induced Polarization

Induced polarization (IP) is a geophysical electrical technique for measuring the electrical impedance of the subsurface. In the frequency domain, two electrodes inject a sinusoidal current into the ground, while another pair of electrodes measures the resulting phase-shifted voltage. The electrical impedance is determined by the amplitude ratio and phase-shift between the voltage and current. By conducting measurements at different frequencies, known as spectral IP (SIP), information about the frequency-dependent electrical properties of the subsurface can be obtained.

Electrical impedance Z can be expressed in terms of the magnitude and phase shift angle or as real (R, resistance) and imaginary (X, reactance) components (Equation 3; Lvovich 2012):

$$Z(\omega) = R - iX = |Z(w)|e^{i\varphi(w)} \quad [3]$$

where φ(ω) (Equation 4) represents the phase shift angle in radians:

$$\varphi(\omega) = \arctan(\frac{-X}{R}) \quad [4]$$

The angular frequency is represented by ω, which is calculated as $2\pi f$, where f is the excitation frequency.

The real component of electrical impedance accounts for energy loss associated with conduction, whereas the imaginary part (or phase-shift angle) represents the polarization effect, which can help to identify the unique

relaxation feature of ice, as demonstrated by previous studies. This paper will focus on the imaginary part, the phase shift angle, and the RFE as additional means to distinguish ice from other materials.

Bittelli et al. (2004) investigated the application of dielectric spectroscopy for estimating the presence and content of ice in frozen porous materials. They employed a dielectric mixing model to calculate the proportions of liquid water, ice, air, soil solids based on their dielectric permittivities and that of the bulk material. Measurements of dielectric permittivities were taken across a temperature range of -30 °C to +5 °C at two frequencies using an electrical impedance analyzer. One (25 kHz) close to the relaxation frequency of ice, and another (158 kHz) significantly above were used to detect ice. The approach was tested on three soil samples with varying clay concentrations. The determination of ice content was successful for the loamy sand, but challenges arose for samples with high clay content, due to surface-related effects at low frequencies such as double-layer polarization, surface conduction, and Maxwell-Wagner effects.

Grimm et al. (2015) analyzed dielectric spectra (0.1 Hz to 1 MHz) for 49 firn and ice samples obtained from ice sheets and glaciers. Results revealed two distinct dielectric relaxations, indicating the presence of different crystal populations or zonation in meteoric ice. However, high temperatures, long residence times, or elevated impurity concentrations favoured the development of a single relaxation, suggesting the merging of distinct populations due to annealing. Furthermore, frozen samples from subglacial environments displayed a single relaxation reflecting the composition of the source water. The findings emphasize the importance of multi-frequency methods for distinguishing different types of ice based on their dielectric properties.

Grimm and Stillman (2015) explored the utility of low-frequency electrical resistivity in discerning frozen ground from unfrozen soil in periglacial environments. The research established temperature-dependent relationships between ice volume and RFE through laboratory experiments using samples collected from the US Army Permafrost Tunnel in Fox, Alaska. By comparing data from laboratory and field measurements, they determined an optimal ice temperature of approximately -3 °C. Subsequently, they employed the laboratory derived RFE at this selected temperature to create a detailed ice content map within the tunnel, ranging from 45 to 95% ice volume. The field data exhibited a strong agreement with SIP results.

Stillman et al. (2018) used SIP to infer patterns of relative subsurface ice content in warm permafrost. They utilized tomographic SIP profiles, which revealed distinct ice signatures at depth based on RFE, which is the difference between the low and high-frequency resistivities normalized by the low-frequency value. Measurement in November presented a challenge because a high-conductivity unfrozen layer near the surface persisted.

Mudler et al. (2022) conducted research on detecting ice in permafrost using the high-frequency induced polarization method (HFIP). Their approach relies on Zorin and Ageev (2017) theory, which characterizes subsurface material as a combination of two components: ice and a ice-free part of the soil. The underlying assumption in this theory is that polarization is exclusively attributed to the ice fraction.

3 Field Observations

3.1 SIP measurements

SIP measurements were made on a pingo site (60.7835°N 137.5321°W) in Haines Junction, Yukon, Canada from 20–22 March, 2023. Throughout this time, the local air temperature varied between -2 °C in the morning to +4 °C in the evening.

A FUCHS III+ device was utilized, operating in the frequency domain and having a maximum current and voltage of 1.5 A and 400 V. It employs sinusoidal current for electrical impedance measurement and records, analyzes, and processes current and voltage signals in real-time, recording and displaying electrical impedance and phase shift angle spectra. It consists of a single current unit and three potential units, with one potential unit designated as the reference for suppressing local noise. Calibration was performed prior to the measurements following a manual procedure. We recorded 582 electrode configurations at 20 frequencies from 1.46 Hz to 40 kHz, resulting in 11,640 data points total at the pingo site.

We measured a survey line that spanned 30 m with electrodes one metre apart. The line was selected to be straight and wide enough for movement of persons and equipment. A geofabric ground cover was used to enable smooth movement of fibreoptic cables. We measured in dipole-dipole configuration with electrode spacings of 1–5 m and using ground electrodes placed in the center of these electrodes.

3.2 Drilling

A borehole was drilled at the 23-m mark within the SIP profile (60.783670º N, 137.53188º W) on April 5, 2023. The borehole reached a depth of approximately 11 m and the recovered core was logged and photographed in the field.

4 Data Processing

This paper focuses solely on the observations at the lowest (1.46 Hz) and highest (40 kHz) measured frequency. We excluded data points displaying negative electrical impedance magnitude and/or positive phase shift angle. Subsequently, we removed observations that were more than three standard deviations away from the mean of all measurements in each frequency, in either electrical impedance magnitude or phase shift angle.

Table 1 presents descriptive statistics for electrical impedance magnitude (IM) and phase shift angle (PA) at 40 kHz and 1.46 Hz, respectively. At 40 kHz, we excluded 16 and 28 data points for electrical impedance magnitude and phase shift angle, respectively. Similarly, at 1.46 Hz, we excluded 11 and 232 data points for electrical impedance magnitude and phase shift angle, respectively. No outlier was found for PA at 40 kHz.

Table 1. Summary of raw and filtered data (after excluding negative electrical impedance magnitude and positive phase angle) for electrical impedance magnitude (Ω) and phase shift angle (degree).

Variable	Count	Mean	StDev	Min	Max
IM (40 kHz)	582	2.55	13.36	0.02	192
IM (40 kHz Filtered)	566	0.94	1.34	0.03	8
IM (1.46 Hz)	582	3.06	18.59	0.03	336
IM (1.46Hz Filtered)	571	1.20	1.84	0.03	15
PA (1.46 Hz)	384	-2.04	5.45	-48.00	0
PA (1.46Hz Filtered)	350	-0.63	0.97	-5.20	0
PA (40 kHz filtered and unfiltered)	554	-10.99	5.82	-40.96	0

After data cleaning, ResIPy was used for inverting the SIP data. This software package has been developed for the inversion of geoelectrical data obtained from ERT and induced polarization (IP) surveys (Blanchy et al. 2020).

Considering the real part of electrical impedance and change it to apparent resistivity (Ωm) values (by using geometric factor) at the lowest (1.46 Hz) and highest (40 kHz) frequencies, we can use Equation 5 for RFE, where a value close to 1 indicates higher ice content (Grimm and Stillman 2015).

$$RFE = (\rho_{1.46Hz} - \rho_{40kHz}) / \rho_{1.46Hz} \quad [5]$$

Where ρ shows the apparent resistivity.

Additionally, we employed the loss tangent to track the relative variation in the imaginary component of electrical impedance. Termed as tan delta, the loss tangent is defined as the ratio of the imaginary part to the real part (Equation 6).

$$Loss\ tangent = \frac{Imaginary\ part\ (X)}{Real\ part\ (R)} \quad [6]$$

5 SIP Results and Interpretation

Figure 2 shows inverted electrical impedance magnitude (RMS 6%) and phase shift angle at 40 kHz (RMS 19 mrad). The electrical impedance magnitude plot uncovers the existence of a high resistivity layer situated approximately 2 m below the surface, spanning a horizontal distance of 22 to 24 m. Additionally, a distinct high resistive layer is observed within a horizontal range of 12 to 20 m.

The area with high resistivity can indicate the presence of various materials, such as ice and bedrock, that possess high resistivity properties. However, it is not possible to draw a definitive conclusion about the presence of ice solely based on resistivity measurements. To enhance the interpretation process, the study examined the results of phase shift angle inversion.

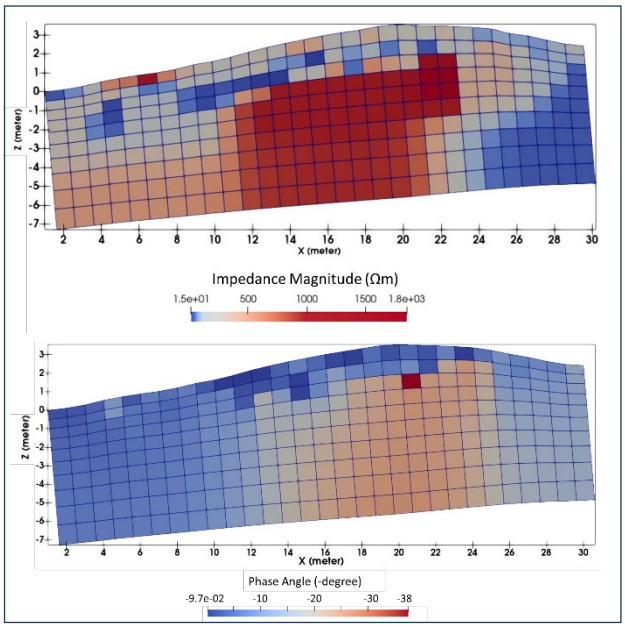

Figure 2. Electrical impedance magnitude (Ωm) and phase angle (degree) at 40 kHz.

The phase shift angle plot revealed higher negative phase values between 14 and 26 m, suggesting a positive correlation with the high resistivity area. Still, it's essential to recognize that this correlation is a sign of the existence of ice, not a definitive proof.

Using Equation 3 we can translate electrical impedance into real and imaginary components. Figure 3 illustrates both the real and imaginary components of the electrical impedance within the study area, at 40 kHz. Directing our attention to the imaginary part of the electrical impedance, it becomes evident that a clearly discernible high resistivity region is located at a depth of ~1.5 m, spanning a horizontal distance between 22 and 27 m. The imaginary part of the electrical impedance, also known as capacitive reactance (X), provides valuable insights into the presence of inductive or capacitive materials. Notably, the negative values of the phase shift angle indicate the presence of capacitive materials. Furthermore, the polarization observed in the imaginary plot (Figure 3) directly correlates with the existence of ice. Therefore, the elevated values observed in the imaginary plot (indicated by the arrows) suggest the possible presence of ice within the study area. Furthermore, the higher values observed at the surface can be attributed to the presence of snow cover.

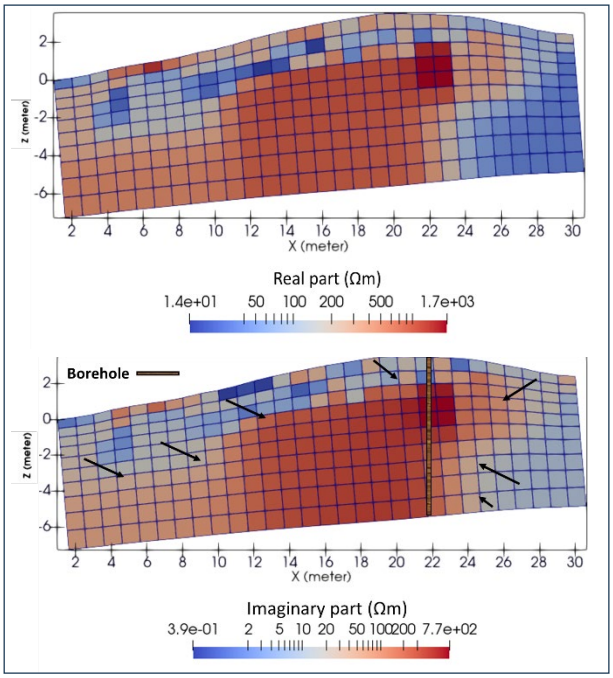

Figure 3. Real and Imaginary part (Capacitance Reactance) of electrical impedance at 40 kHz (the arrows show the elevated values observed in the imaginary plot).

The electrical impedance amplitude (RMS 2%) and phase shift angle (RMS 29 mrad) inversion results at 1.46 Hz are presented in Figure 4. The electrical impedance magnitude plot exhibits similarities with the one at 40 kHz; however, the magnitudes of these two plots differ significantly.

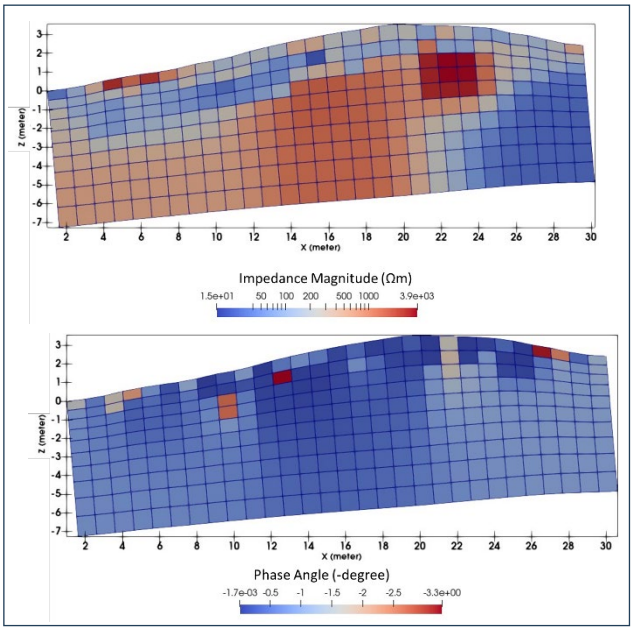

Figure 4. Electrical impedance magnitude, and phase shift angles at 1.46 Hz.

Notably, the resistivity at 1.46 Hz is higher compared to 40 kHz. It's noteworthy that ice polarization is expected within the kHz range. This anticipation is evident in the 40kHz plot, where the phase shift angle exhibits higher values, in contrast to the 1.46Hz plot where it remains below -4°. This contrast serves as a robust indicator of ice polarization.

Figure 5 shows RFE (Equation 5) image for the study area. The higher values correspond to a higher ice content. The red pixels in RFE plot shows higher ice content that is almost compatible with the electrical impedance inversion results at 40 kHz (Figure 3); there are some unanticipated differences among them that can be explained by the presence of clay in the study area especially when the presence of clay affects the real part resistivity values in the highest and the lowest frequencies.

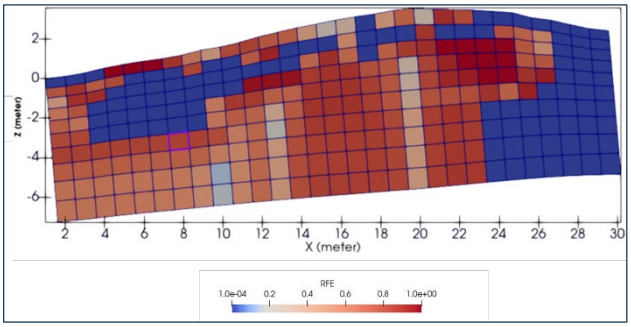

Figure 5. RFE result for the study area.

6 Comparison with Drill Logs

The borehole log (Table 2; 60.7837°N 137.53188°W; Figure 3) reveals fibric organics, including mosses and wood fragments near the surface (0–0.1 m) and subsequent layers (0.1–0.3 m) are composed of notably dry and dense silt. An air-filled void (0.3–0.6 m) is associated with cracking at the pingo's apex. Clayey silt (1.25–2.4 m) displays 5% visible ice volume and the silty clay below features increasingly prominent ice lenses. The most significant ice body (3.6–8.3 m; Figure 6) has a visible ice content of 98%. Notably, sporadic lenses of silty clay transition into diamict lenses as depth increases, with thicknesses ranging from 5 to 20 cm. Below 8.3 m, there is a water-filled section with an uncertain composition of either gravel or diamict.

Figure 7 displays variations in the phase shift angle at the borehole location. It reveals a low phase shift angle value of -2.83° in the ice-free zone at a depth of 0–0.6 m. With the presence of ice, there is a slight change from -2.83 to -2.87° at 0.6 m, aligning with the boundary between the clayey silt (lower ice content) and air layer (ice-free layer). In the middle of this layer (1.5 m), the phase shift angle experiences a significant shift, reaching -24.2° likely due to ice polarization. At 2.2 m depth, another change occurs, marking the boundary between silty clay and clayey silt with higher ice content. From a depth of 3.6 to 8.3 m, the increasing ice volume results in gradual shifts toward more negative phase shift angle values, reaching -25.2° at 8.3 m depth. The initial phase shift angle change for the last layer occurs at 4.7 m depth, approximately one meter away from

the boundary between the ice layer and silty clay, possibly due to the lower resolution of 40 kHz at greater depths.

Table 2. Log details for borehole on pingo. Ice content is given in estimated volume percent of visible ice.

Depth (m)	Material	Frozen	Ice (%)	Ice
0–0.1	Fibric organics	Y	Nil	Nf
0.1–0.3	Silt	Y	Nil	Nf
0.3–0.6	Air		Nil	-
0.6–2.4	Clayey silt	Y	5	Vx
2.4–2.9	Silty clay	Y	20	Vr
2.9–3.6	Silty clay	Y	30	Vr
3.6–8.3	Ice	Y	98	ICE+clay +diamict
8.3–10.8	Gravel	N	0	-

Figure 6. Core recovered from 6.0 to 6.6 meters depth.

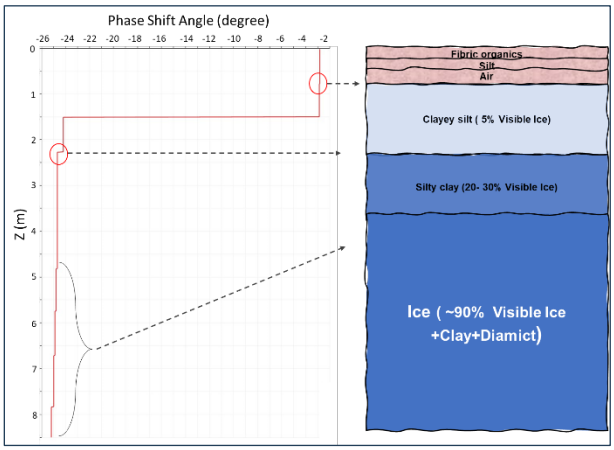

Figure 7. Phase Shift Angle at 40 kHz (extracted for the borehole location).

Figure 8 illustrates changes in electrical impedance magnitude, real and imaginary part (on the left side), as well as the loss tangent (on the right side). In the ice-free layers, the imaginary part remains stable at around 1.6 Ωm. However, at a depth of 1.5 m, these values significantly increase to 500 Ωm due to the presence of icy clayey silt layers. In the upper depth (ice-free layer), the real part is nearly equal to the electrical impedance magnitude, with a ratio close to 1. Conversely, within the ice layer, the real part contributes less to the electrical impedance magnitude, while the imaginary part takes on a more significant role (loss tangent reaching up to 0.47 at a depth of 8.3 m). Despite decreasing resistivity values at greater depths (due to clay present), the increasing ice content results in a higher loss tangent, as the contribution of the real part decreases.

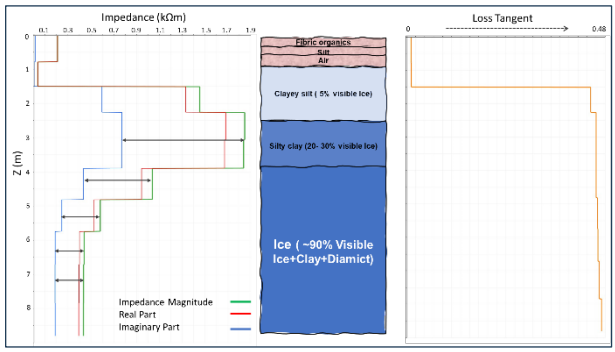

Figure 8. Electrical impedance magnitude, real, imaginary part, and loss tangent at 40 kHz (extracted for the borehole location).

7 CONCLUSIONS

This study effectively utilized Spectral Induced Polarization (SIP) to identify the ice core at the pingo site located in Haines Junction, Yukon province. The data acquisition process involved utilizing the FUCHS frequency domain instrument across a frequency spectrum ranging from 1.46 Hz to 40 kHz. At 1.46 Hz (Figure 4), the phase angle exhibited low values, indicating that the capacitance had dissipated, allowing electrical energy to flow entirely through the resistive pathway. Conversely, the phase shift angle (and imaginary part of electrical impedance) at 40 kHz (Figures 2 and 3) showed high values due to the presence of ice, aligning with the high ice volume observed in the borehole. Additionally, the RFE equation was applied to detect the core ice. While higher RFE values reliably indicated the presence of ice, the existence of clay (free ions) complicated the relationship between RFE and ice content. For the next study, the focus will be on extracting dielectric spectra across all 20 frequencies and comprehensively analyzing the relationship between ice content, water content, and temperature within the SIP data.

8 ACKNOWLEDGEMENTS

This work would not have been possible without the help of Moya Painter, and Patrick Sack.

Funding for this field campaign came from the Yukon Geological Survey, and Natural Science and Engineering Research Council of Canada (NSERC). This is Yukon Geological Survey contribution 065.

9 REFERENCES

Artemov, V.G. and Volkov, A.A. 2014. 'Water and ice dielectric spectra scaling at 0°C', *Ferroelectrics* 466(1), pp. 158–165. doi:10.1080/00150193.2014.895216.

Bittelli, M., Flury, M., and Roth, K. 2004. 'Use of dielectric spectroscopy to estimate ice content in frozen porous media', *Water Resources Research* 40(4). doi:10.1029/2003WR002343.

Blanchy, G., Saneiyan, S., Boyd, J., McLachlan, P., and Binley, A. 2020. 'ResIPy, an intuitive open source software for complex geoelectrical inversion/modeling', *Computers and Geosciences* 137. doi:10.1016/j.cageo.2020.104423.

Grimm, R.E. and Stillman, D.E. 2015. 'Field test of detection and characterisation of subsurface ice using broadband spectral-induced polarisation', *Permafrost and Periglacial Processes* 26(1), pp. 28–38. doi:10.1002/ppp.1833.

Grimm, R.E., Stillman, D.E., and MacGregor, J.A. 2015. 'Dielectric signatures and evolution of glacier ice', *Journal of Glaciology* 61(230), pp. 1159–1170. doi:10.3189/2015JoG15J113.

Grimnes, S. and Martinsen, Ø.G. 2015. 'Electrolytics', *Bioimpedance and Bioelectricity Basics*, pp. 9–36. doi:10.1016/B978-0-12-411470-8.00002-7.

Hobbs, P.V. 2010. *Ice physics*. Oxford, England: Oxford University Press.

Kasprzak, M., Strzelecki, M.C., Traczyk, A., Kondracka, M., Lim, M., and Migała, K. 2017. 'On the potential for a bottom active layer below coastal permafrost: the impact of seawater on permafrost degradation imaged by electrical resistivity tomography (Hornsund, SW Spitsbergen)', *Geomorphology* 293, pp. 347–359. doi:10.1016/j.geomorph.2016.06.013.

Kemna, A., Binley, A., Cassiani, G., Niederleithinger, E., Revil, A., Slater, L., Williams, K.H., Orozco, A.F., Haegel, F.H., Hördt, A., Kruschwitz, S., Leroux, V., Titov, K., and Zimmermann, E. 2012. 'An overview of the spectral induced polarization method for near-surface applications', *Near Surface Geophysics* 10(6), pp. 453–468.

Li, X., Jin, X., Wang, X., Jin, H., Tang, L., Li, X., He, R., Li, Y., Huang, C., and Zhang, S. 2021. 'Investigation of permafrost engineering geological environment with electrical resistivity tomography: A case study along the China-Russia crude oil pipelines', *Engineering Geology* 291. doi:10.1016/j.enggeo.2021.106237.

Lvovich, V.F. 2012. *Impedance spectroscopy: applications to electrochemical and dielectric phenomena*. Hoboken, New Jersey, United States: John Wiley & Sons.

Mudler, J., Hördt, A., Kreith, D., Sugand, M., Bazhin, K., Lebedeva, L., and Radić, T. 2022. 'Broadband spectral induced polarization for the detection of Permafrost and an approach to ice content estimation - a case study from Yakutia, Russia', *Cryosphere* 16(11), pp. 4727–4744. doi:10.5194/tc-16-4727-2022.

Oldenborger, G.A. 2021. 'Subzero temperature dependence of electrical conductivity for permafrost geophysics', *Cold Regions Science and Technology* 182. doi:10.1016/j.coldregions.2020.103214.

Park, K., Kim, K., Kim, K., and Hong, W.T. 2023. 'Characterization of active layer at different degrees of patterned ground development using electrical resistivity tomography survey', *Cold Regions Science and Technology* 208. doi:10.1016/j.coldregions.2022.103734.

Petrenko, V.F. and Whitworth, R.W. 1999. *Physics of ice*. Oxford, England: Clarendon Press.

Stillman, D.E., Grimm, R.E., and Gruber, S. 2018. 'Spectral induced polarization surveys to infer ground ice in a peatland and a lithalsa in warm permafrost near Yellowknife, Canada', in *5th European Conference on Permafrost: Extended abstracts*. Chamonix-Mont Blanc, France: pp. 1–2.

You, Y., Yu, Q., Pan, X., Wang, X., and Guo, L. 2013. 'Application of electrical resistivity tomography in investigating depth of permafrost base and permafrost structure in Tibetan Plateau', *Cold Regions Science and Technology* 87, pp. 19–26. doi:10.1016/j.coldregions.2012.11.004.

Zorin, N. and Ageev, D. 2017. 'Electrical properties of two-component mixtures and their application to high-frequency IP exploration of permafrost', *Near Surface Geophysics* 15(6), pp. 603–613.